Multilayer Films from Templated TiO_2 and Structural Changes during their Thermal Treatment

Jan Procházka,*,† Ladislav Kavan,† Valery Shklover,‡ Markéta Zukalová,‡ Otakar Frank,† Martin Kalbáč,† Arnošt Zukal,† Hana Pelouchová,† Pavel Janda,† Karel Mocek,† Mariana Klementová,§ and Dina Carbone||

J. Heyrovsky Institute of Physical Chemistry of the Academy of Sciences of the Czech Republic, v.v.i, Dolejškova 3, CZ-18223-Prague 8, Czech Republic, Laboratory of Crystallography, Department of Materials, ETH Hönggerberg, Wolfgang-Pauli-Strasse 10, CH-8093 Zürich, Switzerland, Institute of Inorganic Chemistry of the Academy of Sciences of the Czech Republic, v.v.i, CZ-250 68 Řež near Prague, Czech Republic, and ESRF Grenoble, 38043 Grenoble Cedex, France

Received May 29, 2007. Revised Manuscript Received December 7, 2007

This work is focused on synthesis, characterization, and determination of main parameters of the multilayer P123 templated TiO_2 films. The mesoporous multilayer thin films consist of TiO_2 nanoparticles on the F-doped SnO_2 (FTO) conductive glass substrates. The films were grown by implementing the protocol of supramolecular templating with the amphiphilic triblock copolymer, Pluronic P123. The templated multilayer films were manufactured by repeated dip coating followed by the thermal treatment at 350 °C for 2 h after deposition of each layer. It was found that the multilayer preparation technique at 350 °C has serious limitations. The structure does not further increase its specific surface area (roughness factor) after deposition of more than 3−5 layers. The new surface area added by deposition of the top layer is compensated by the reduction of the surface area lost due to the sintering of the bottom layers. The careful review of the analytical data suggests that the morphology of the P123 templated TiO_2 structure is likely the tightest arrangement of randomly positioned particles of a certain size on a given pore diameter. The bulk material consists of pores evenly formed in all directions while a denser crust is formed on the surface where the fusion was restricted in one direction at the interface with the air. Subsequent thermal treatments of the multilayer films were applied to improve the anatase crystallinity while keeping the open morphology and small particle size. The morphological changes of the mesoporous structure during the subsequent thermal treatment at 425−540 °C were investigated.

1. Introduction

The mesoporous network of TiO_2 nanoparticles is used in many applications such as solar cells, photocatalysis, or electrochromic and light-emitting devices. Considerable effort has been spent on the development of TiO_2 mesoporous thin films consisting of ultrasmall particles. The high-quality transparent mesoporous TiO_2 films on F-doped tin oxide conducting glass (FTO) are applicable for solar cells based on the spectral sensitization of titanium dioxide (anatase) to visible light (Grätzel cell).[1–3]

The past few years have been in a sign of systematic research effort to prepare sophisticated organized TiO_2 structures. Stucky et al.[4–6] have discovered a promising strategy using amphiphilic triblock copolymers (Pluronic) as the structure-directing agents. This synthetic protocol was further developed by Ozin et al.,[7] Sanchez et al.,[8] and Smarsly et al.[9] We have further upgraded this strategy by a reproducible scaling up of the film thickness. Highly efficient TiO_2 electrodes of ca. 1 μm film thickness were fabricated for the Grätzel cell via triple layer-by-layer deposition.[10] The promising performance of Pluronic-templated TiO_2 in the liquid-junction[11] and the solid-state Grätzel cell[12] were also confirmed by other laboratories. Thin films of mesoporous TiO_2 were grown by dip coating via a procedure called

* Corresponding author.
† J. Heyrovsky Institute of Physical Chemistry of the Academy of Sciences of the Czech Republic.
‡ ETH Hönggerberg.
§ Institute of Inorganic Chemistry of the Academy of Sciences of the Czech Republic.
|| ESRF Grenoble.

(1) Wu, N. L.; Wang, S. Y.; Rusakova, I. A. *Science* **1999**, *285*, 1375.
(2) Grätzel, M. *Nature* **2001**, *414*, 338.
(3) Grätzel, M. *Chem. Lett.* **2005**, *34*, 8.
(4) Yang, P.; Zhao, D.; Margolese, D. I.; Chmelka, B. F.; Stucky, G. D. *Nature* **1998**, *396*, 152.
(5) Yang, P.; Zhao, D.; Margolese, D. I.; Chmelka, B. F.; Stucky, G. D. *Chem. Mater.* **1999**, *11*, 2813.
(6) Alberius, P. C. A.; Frindell, K. L.; Hayward, R. C.; Kramer, E. J.; Stucky, G. D.; Chmelka, B. F. *Chem. Mater.* **2002**, *14*, 3284.
(7) Choi, S. Y.; Mamak, M.; Coombs, N.; Chopra, N.; Ozin, G. A. *Adv. Funct. Mater.* **2004**, *14*, 335.
(8) Crepaldi, E. L.; Soler-Illia, G. J. A. A.; Grosso, D.; Cagnol, F.; Ribot, F.; Sanchez, C. *J. Am. Chem. Soc.* **2003**, *125*, 9770.
(9) Fattakhova-Rohlfing, D.; Wark, M.; Brezesinski, T.; Smarsly, B. M.; Rathousky, J. *Adv. Funct. Mater.* **2007**, *17*, 123.
(10) Zukalova, M.; Zukal, A.; Kavan, L.; Nazeeruddin, M. K.; Liska, P.; Grätzel, M. *Nano Lett.* **2005**, *5*, 1789.
(11) Hou, K.; Tian, B.; Li, F.; Bian, Z.; Zhao, D.; Huang, C. *J. Mater. Chem.* **2005**, *15*, 2414.
(12) Lancelle-Beltran, E.; Prene, P.; Boscher, C.; Belleville, P.; Buvat, P.; Lambert, S.; Guillet, F.; Boissiere, C.; Grosso, D.; Sanchez, C. *Chem. Mater.* **2006**, *18*, 6152.
(13) Brinker, C. J.; Sellinger, H.; Fan, J. *Adv. Mater.* **1999**, *11*, 579.
(14) Boettcher, S. W.; Bartl, M. H.; Hu, J. G.; Stucky, G. D. *J. Am. Chem. Soc.* **2005**, *127*, 9721.
(15) Grosso, D.; Cagnol, F.; Soller-Illia, G. J. A. A.; Crepaldi, E. L.; Amenitsch, H.; Brunet-Bruneau, A.; Bourgeois, A.; Sanchez, C. *Adv. Funct. Mater.* **2004**, *14*, 309.

10.1021/cm071452e CCC: $40.75
Published on Web 04/12/2008

evaporation-induced self-assembly (EISA).[13–15] The film quality was significantly influenced by experimental conditions, such as ambient humidity, withdrawal rate, type of titania precursor, and solvent.[6,7,16,17]

Nearly all of the above-mentioned applications require large surface area and well developed crystallinity of the nanoanatase with the particles organized in a highly porous structure. However, TiO_2 fabricated via supramolecular templating with Pluronic contains a significant amount of amorphous titania[4–6,8] in which anatase nanocrystals are embedded. Other phases beyond anatase were not reported very frequently, but Sanchez et al.[8] found brookite, which grew somewhat unexpectedly by thermal transformation of anatase in small-size inorganic domains. Zukalova et al.[18] newly found small amounts of monoclinic TiO_2(B) in these materials. Recently, Smarsly et al.[9] also confirmed the presence of TiO_2(B) in the Pluronic-templated materials. They also reported that the content of amorphous titania was between 40 and 60 mol% depending on the calcination temperature, while phase pure anatase was obtained after calcination at 600 °C.[9] Both the quantitative determination of amorphous TiO_2 and the detection of TiO_2(B) was carried out via electrochemical methods.[9,18]

The crystallinity of TiO_2 film can be improved by a high temperature thermal treatment. However, it is accompanied by fusing, particle size growth, and, eventually, collapse of the structure. This study is focused on optimalization of the thermal treatment with respect to the surface area and crystallinity of the nanoanatase mesoporous films. We have systematically optimized the manufacturing of the multilayer films up to 2.3 μm thickness by extending the protocol of layer-by-layer deposition[10,19] up to ten layers. It is believed that the P123 micelles plug the pores of the previously created layer stopping the TiO_2 particles from penetrating into the mesoporous structure. The plugging effect allows smooth deposition of another layer on the top of the previous one without significant changes in the density of the multilayer film. In addition, we have probably found the natural limit of the achievable increase of the TiO_2 surface area (roughness factor) in these films.

Single-layer Pluronic templated TiO_2 films were frequently characterized by electron microscopy (SEM and TEM) and small-angle X-ray scattering using classical X-ray sources such as CuK.[6–8,14,16] We have combined various microscopic and diffraction techniques to follow the structural changes in our multilayer mesoporous films. In addition to the electron and scanning probe microscopy methods, the structure of our films was analyzed using the grazing-incidence small-angle X-ray scattering (GISAXS) with 10 keV synchrotron radiation beam source providing us valuable statistical data about the structure.

2. Experimental Section

2.1. Materials. The TiO_2 films were grown from a suspension made by the addition of 9.7 g of HCl (37% Aldrich) to 12.7 g of titanium ethoxide (Aldrich) under vigorous stirring. Separately, 4.0 g of block copolymer Pluronic P123 [$OH(CH_2CH_2O)_{20}(CH_2CH(CH_3)O)_{70}(CH_2CH_2O)_{20}H$] from Aldrich was dissolved in 36.3 g of 1-butanol (Aldrich) and added to the HCl/$Ti(EtO)_4$ suspension. This suspension was aged by stirring at ambient temperature for at least 3 h. The films were deposited by dip coating (withdrawal rate of 0.8 mm/s) onto 5.0 × 1.3 cm sized slides of F-doped SnO_2 glass slides (TEC 8 from Libbey-Owens-Ford, 8 Ω/square; further abbreviated FTO). For this purpose, we have used a homemade setup for vibration-free dip-coating. It consisted of a hydraulic piston, which was operated by a precision pump (KD Scientific, USA). The layer was aged at 75% relative humidity and 24−25 °C temperature for 24 h. Next, the layer was calcined in the air at 350 °C for 2 h (heating rate: 1 °C/min). Thicker films consisting of more layers were prepared by repeating the procedure up to ten times. In addition to the pure TiO_2 films, proprietary doped P123 precursors were used to inhibit the particle size growth.

These multilayer films were then thermally treated at temperatures 425−540 °C for 1−8 h to promote the anatase crystal phase development. All thermal treatments occurred in the air with the ramp rate between 1 and 30 °C/min. The slow ramp was typically 3 °C/min, and the fast ramp was 30 °C/min. A series of over 100 samples was prepared for characterization and selected analyses. All the prepared TiO_2 films were crackfree and optically transparent. The film thickness was linearly proportional to the number of layers even after the subsequent thermal treatment (STT). In contrast to the literature,[9] no one-direction collapse of the TiO_2 structure occurred upon heating.

2.2. Characterization Methods. The specific surface area is expressed by the roughness factor (RF), which is the physical surface area of the TiO_2 electrode divided by the projected electrode area. Adsorption isotherms of krypton at 77 K were measured using the Micromeritics ASAP 2020 instrument. Before the adsorption measurement all samples were degassed at 523 K overnight. The BET surface area was calculated using the data in the range of the relative pressure p/p_0 from 0.05 to 0.25. Following the usual practice, the saturation vapor pressure p_0 of the supercooled liquid krypton and the atomic cross-sectional area of 0.21 nm^2 were used. The surface area of TiO_2 was normalized per one square centimeter, so the roughness factor values were obtained. The film thickness was measured by the alpha-step profilometer, Tencor Instruments. Scanning electron microscopy (SEM) images were acquired at the Hitachi FE SEM S-4800 microscope. Transmission electron microscopy (TEM) was performed using the JEOL JEM 3010 microscope operating at 300 kV (LaB_6 cathode, point resolution 1.7 Å). Images were recorded by a CCD camera with resolution of 1024 × 1024 pixels using the Digital Micrograph software package. Powder samples were dispersed in ethanol and the suspension was sonicated for 10 min. A drop of very dilute suspension was placed on a carbon-coated grid and allowed to evaporate at ambient temperature. Atomic force microscopic (AFM) characterization and imaging were carried out using the Nanoscope IIIa Multimode Atomic Force Microscope (Veeco, USA) operating in the tapping mode with silicone cantilevers (OTESPA, Veeco, USA).

Grazing incidence small-angle X-ray scattering (GISAXS) measurements were carried out at the ID1 unit of the Grenoble

(16) Coakley, K. M.; Liu, Y.; McGehee, M. D.; Frindell, K. L.; Stucky, G. D. *Adv. Funct. Mater.* **2003**, *13*, 301.
(17) Bartl, M. H.; Boettcher, S. W.; Hu, E. L.; Stucky, G. D. *J. Am. Chem. Soc.* **2004**, *126*, 10826.
(18) Zukalova, M.; Kalbac, M.; Kavan, L.; Exnar, I.; Grätzel, M. *Chem. Mater.* **2005**, *17*, 1248.
(19) Zukalova, M.; Prochazka, J.; Zukal, A.; Yum, J. H.; Kavan, L. *Inorg. Chim. Acta* **2008**, *361*, 656.
(20) Metzger, T. H.; Kegel, I.; Paniago, R.; Lorke, A.; Peisl, J.; Schulze, J.; Eisele, I.; Schittenhelm, P.; Abstreiter, G. *Thin Solid Films* **1998**, *336*, 1.

Table 1. Five Layer P123 Templated TiO_2 Film: Parameters before and after STT

	physical characteristics			GISAXS					
						multimode porosity			TiO_2 primary particle size (nm)
sample	roughness factor	TiO_2 film thickness (μm)	anatase crystal phase (%)	critical incident angle (deg)	Ex-P123 pore size (nm)	max 1 (nm)	max 2 (nm)	max 3 (nm)	
five-layer film (5L)	429	1.3	50	0.13	20	6.4	5.6	4.7	8 to10
5 L 425 °C for 8 h	328	1.3	80−90	0.132	15	6.8	5.7	4.8	11 to 12
5 L 540 °C for 1 h	96	1.3	100	0.13	27−45	17	10	6.1	20 to 40

ESRF facility using 10 keV beam. A position sensitive detector placed along the direction perpendicular to the sample surface was used, in a way that during the GISAXS acquisition a Q_x-Q_z map could be acquired in one scan, or the intensity integrated on the whole detector (about 2°).

GISAXS is a nondestructive and depth-sensitive technique, which are the main points of strength of this method. It is possible to get information about buried layers at different depth from the surface, without need of destroying the sample. With respect to imaging methods, like AFM, SEM, or TEM, which are local techniques, GISAXS provides a better statistical sampling over large areas of the sample, with higher accuracy for extracting average values of morphological parameters of the surface, such as average size of particles and pores of the structure, or their average distance which, in case of closely packed structures, will coincide.

Generally the GISAXS scans are shown in Q space. This is done using the simple relations:

$$Q_x = 2\pi \sin(\Theta)/\lambda, \quad \text{and} \quad Q_z = 2\pi \sin(\Theta_{PSD})/\lambda$$

Where, λ is the radiation wavelength (1.2397 Å), Θ is the diffraction angle, and Θ_{PSD} is the angle along the PSD detector. The GISAXS intensity is dominated by the form factor of the near-surface structures and their lateral correlation. The form factor is related to the structure size and shape,[20] and is concentrated in the region $Q_x = 0$ of the reciprocal space. The lateral correlation appears in the GISAXS profiles as the intensity maxima at position $Q_x \neq 0$ symmetrical with respect to the origin. The large size dispersion of the surface structures makes the GISAXS profiles scarcely sensitive to the average form factor and dominated, instead, by the spatial correlation of the nanostructures (i.e., average distance between particles/pores) which can be extracted by a simple formula

$$D = 2\pi/Q_x$$

The relative density of the film was determined from the critical angle values of the reflectivity scans. The beam penetrated more than one layer at 0.4° indicating a very porous structure. Exclusion method was used to associate the peaks on the GISAXS patterns with the particle size values and different pore types (Table 1). Reference data for this exclusion were obtained by the analytical methods described in this section. The coherent domain size of TiO_2 particles was calculated from diffraction patterns of wide-angle X-ray scattering (WAXS) using the Scherrer equation.

Electrochemical lithium insertion was studied by cyclic voltammetry using the Autolab PGSTAT 30 (Ecochemie) potentiostat controlled by a GPES-4 software. The reference and auxiliary electrodes were from Li metal; hence, potentials are referred to the Li/Li^+ (1 M) reference electrode. $LiN(CF_3SO_2)_2$ (Fluorad HQ 115 from 3M) was dried at 130 °C at 1 mPa. Ethylene carbonate (EC) and 1,2-dimethoxyethane (DME) were dried over the 4A molecular sieve (Union Carbide). The electrolyte solution was 1 M $LiN(CF_3SO_2)_2$ + EC/DME (1/1 by volume). All operations were done under argon in a glovebox.

3. Results and Discussion

3.1. Film Morphology of the Bulk, Top Crust, and Individual Layers. Parameters of the multilayerfilms prepared by the modified Stucky's protocol[10] characterized by the above methods differ sometimes from the previously reported numbers.[4–6,8] While there has been a reasonably

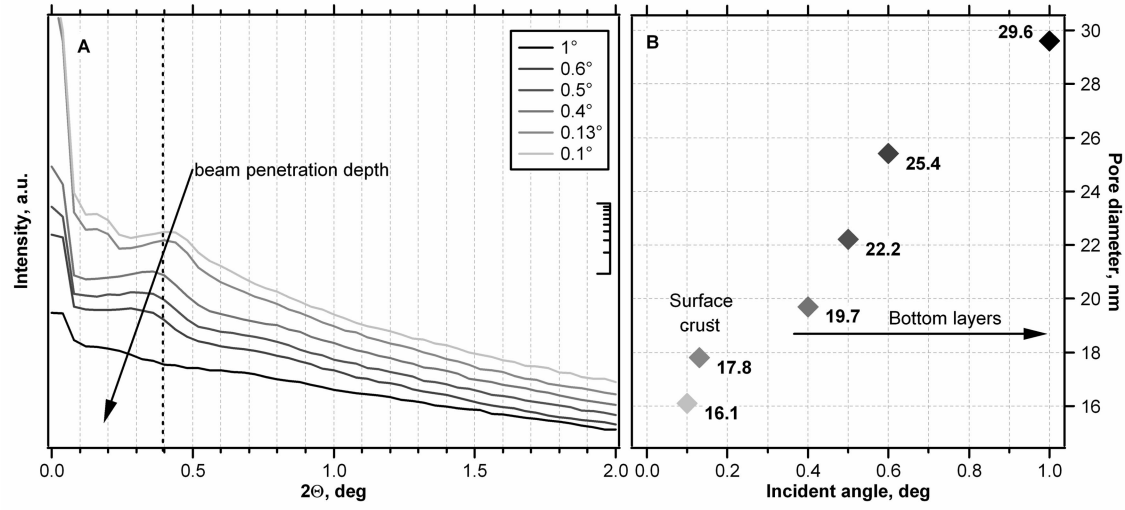

Figure 1. (A) GISAXS measurements: Pore size increase throughout the TiO_2 film from the top to the bottom. The measurements were taken at different incident angles with different penetration depths of the beam. The curves indicate a moving peak around 0.4° associated with the P123 porosity. (B) Summarized results of the 0.4° parameter plotted into a graph showing an increase of the ex-P123 pore size in deep layers. The logarithmic scale bar in part A represents one order of a magnitude of counts per second.

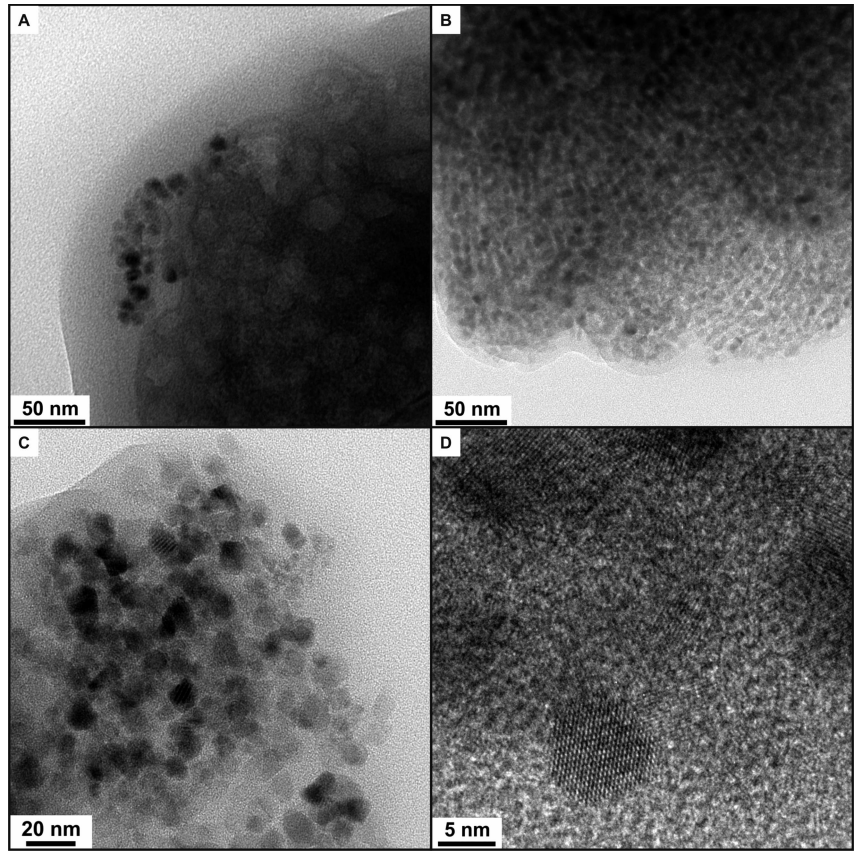

Figure 2. TEM pictures of the basic P123 templated structure before a subsequent thermal treatment: (A) light spots about 20 nm in size show the P123 pore with rather irregular shape left after P123 micelles; (B) organized structure; (C) particle size distribution of a crushed film; (D) average particle size (8−10 nm).

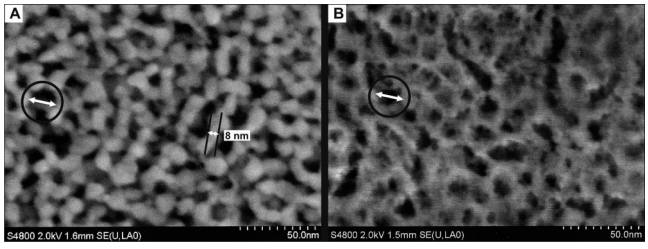

Figure 3. SEM images of templated film before a subsequent thermal treatment: top view. (A) TiO_2 particles 8 nm in diameter surrounding 20 nm P123 pores. (B) Thermally stabilized TiO_2 particles 2−3 nm in diameter surrounding 20 nm P123 pores.

good agreement on the TiO_2 primary particle size (7−10 nm), the pore size values in the literature vary from approximately 7 to 15 nm. Our analysis evidence the presence of even larger pores. They grow from about 20 to 30 nm in the FTO substrate direction (Figure 1) Obviously, the pores open due to the multiple calcination steps at 350 °C causing sintering of the bottom layers after deposition of each additional layer.

Figure 1 shows the ex-P123 pore size development based on the GISAXS information. The individual scans are in Figure 1A, and the results are summarized in part B. The detector accumulates intensity values collected through the entire profile. The position of the 0.4° parameter (indicated by the dashed vertical line) is shifting depending on the penetration depth of the beam. At small incident angles up to 0.2° the penetration depth is less than 20 nm, thus giving information only about the surface. At approximately 0.4°, the beam penetrates through the first layer (250 nm). This top layer has been calcined only once; therefore, we could not see many changes in the 0.1−0.4° incident angle range. There is only a slight difference in GISAXS parameters of the top crust and the pore size in the first layer under it. From 0.4°, the penetration depth rapidly increases to about 1 μm at 1°. On the basis of reference analyses, we have associated the 0.8° GISAXS parameter with the TiO_2 particle size. Comparing the GISAXS maxima, there was just a small increase of the particle size, but a major change of the pore size parameter (0.4°) in the bottom layers.

The structure of the mesoporous film consists of two different morphologies, the ordinary three-dimensional bulk, with a denser top crust on the surface. In the bulk, the particles can grow in any direction (left and right, forward and backward, up and down), while directly on the surface the fusion cannot progress in the interface direction. The crust on the surface was created by the competitive particle growth causing a preferential fusion to the sides at the interface with the air. The crust is parallel to the substrate. It is denser than the unclipped structure underneath.

Typical explanations including that presented in our recent work[10] describe the oriented-like assemblies as a result of self-organization of TiO_2 nanoparticles. This self-organization is supposed to take place as a result of both P123-templating and aging. Since P123 is a nonionic surfactant, the driving force for the micelle forming is believed to be just the difference in hydrophilicity between the polyethylene oxide (PEO) and polypropylene oxide (PPO) chains of the mol-

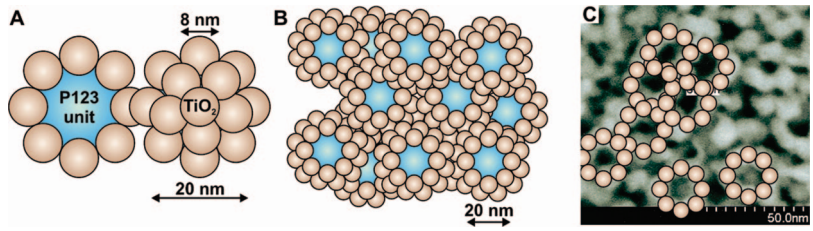

Figure 4. Model of closest packing of 8 nm particles on the 20 nm diameter (A) single unit; (B) top view (crust); and (C) proportional projection of our model onto a real TiO_2 structure.

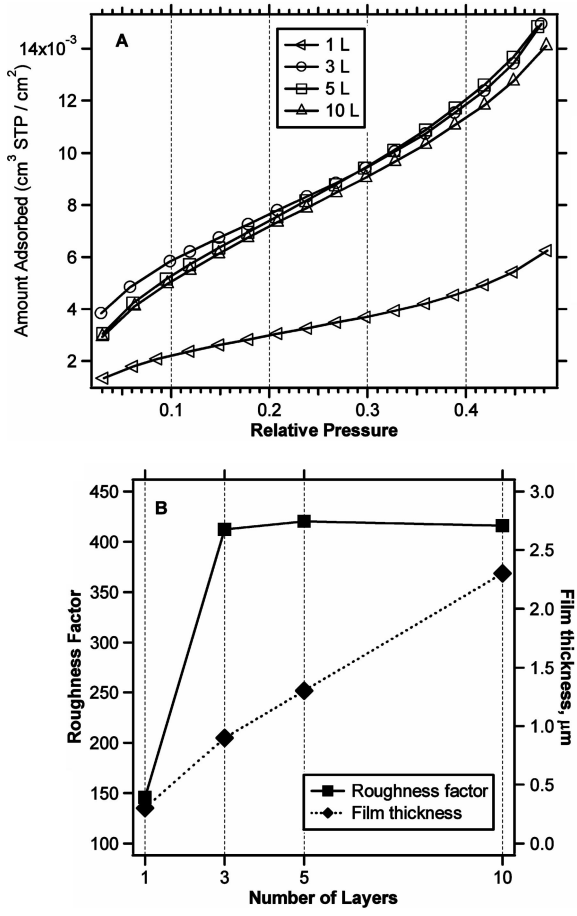

Figure 5. (A) Adsorption isotherms of 1, 3, 5, and 10 layer TiO_2 film. (B) Disproportion in the film thickness and TiO_2 surface area (expressed as roughness factor) during the deposition of individual TiO_2 layers.

ecule. The mesoporous structure is formed as a result of the attractive forces between the titanium dioxide hydrate and P123, followed by crystallization at elevated temperature. Since the binding affinities between the nonionic surfactant and framework material are much weaker compared to those in ionic templates, the resulting porous structure is less ordered. Although some copolymers are able to create an oriented structure, we believe that in the P123 case the limited fusion on the surface has created a geometry looking similar to hexagonal or even decagonal formations. On the basis of our current analyses, it seems that the previously reported self-organized ordered structure of TiO_2 might in fact be the tightest packing of 7−10 nm particles on a pore of 15−25 nm in diameter. The parameters of the structure were determined by number of the above-mentioned methods.

The ex-P123 pore size and shape is obvious from TEM image in Figure 2A. The P123 micelles do not have a regular

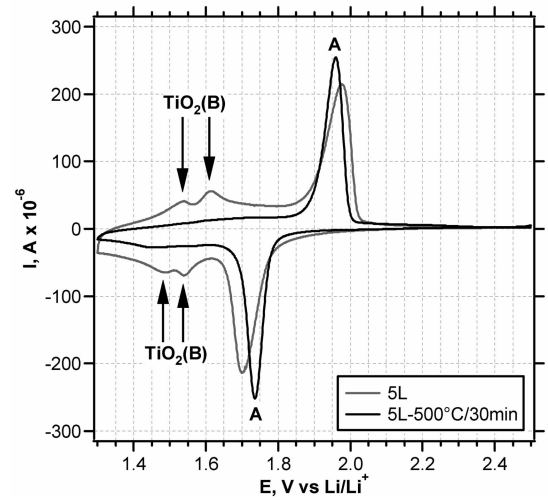

Figure 6. Cyclic voltammograms of Li^+ insertion into TiO_2 at 0.1 mV/s showing the crystal phase development after the subsequent thermal treatment at 500 °C for 30 min. TiO_2(B) and amorphous TiO_2 rapidly convert into the anatase phase at higher temperature.

spherical shape as the Figure 2A indicates. TEM also revealed the frequently reported[6,8,21] organized structure consisting of parallel oriented ropes of TiO_2 particles (Figure 2B). However, the presence of this type of ordering in the bulk of the sample processed at 350 °C was rare. The TiO_2 particle size of 8−10 nm determined from TEM (Figure 2C and D) agrees well with the 0.8° parameter corresponding to 8.9 nm obtained by GISAXS at the critical incident angle scan. This parameter very slightly increases with the penetration depth of the beam.

Figure 3 shows SEM images of two identically prepared P123 templated structures. The sample in Figure 3A consists of pure TiO_2, while the structure in Figure 3B was made of proprietary doped TiO_2 precursor, which inhibited the particle size growth. Plain TiO_2 particles fused to the size about 8 nm. They are situated on approximately 20 nm pores. These pores are imprints of the P123 micelles that were burned off during the thermal processing. The thermally stabilized doped TiO_2 particles only grew up to a size of about 3 nm. They appear to be randomly distributed around the micelles. Obviously, the small particles do not seem to be organized (Figure 3B). The particle organization emerges only after the particles fused together to a certain size (Figure 3A). The ex-micelle pores in the SEM images are roughly spherical, looking similar as in the TEM picture (Figure 2A).

Some of the former interpretations of the small-angle X-ray scattering (SAXS) of the calcined Pluronic-templated TiO_2

(21) Yun, H.; Miyazawa, K.; Zhou, H.; Honma, I.; Kuwabara, M. *Adv. Mater.* **2001**, *13*, 1377.

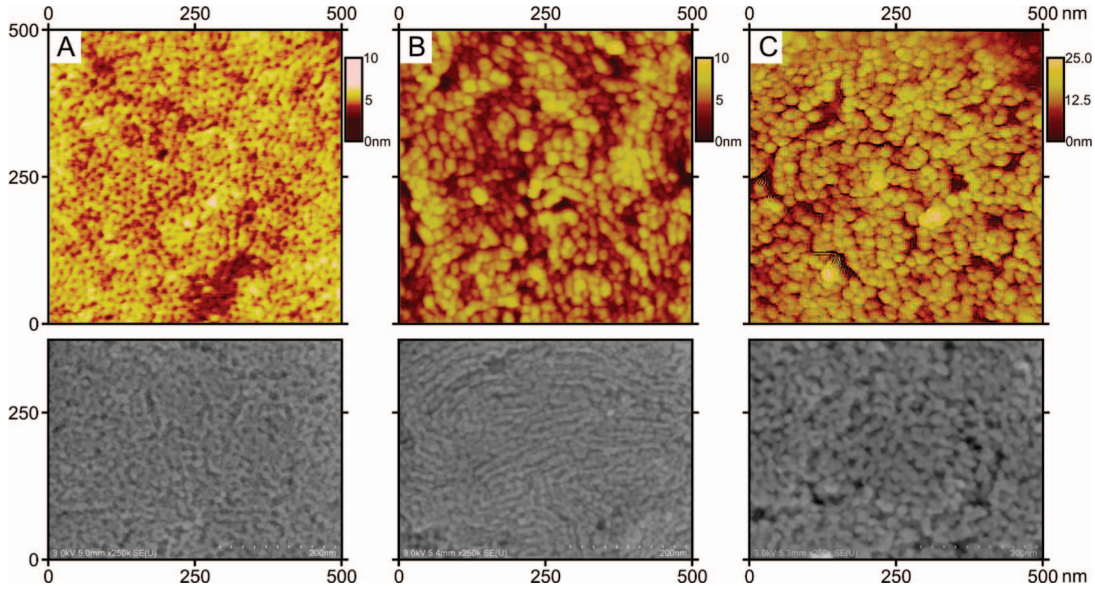

Figure 7. AFM and SEM characterization: Morphology changes of P123 templated five-layer films after the subsequent thermal treatment. (A) No treatment. (B) 425 °C for 8 h. (C) 540 °C for 1 h.

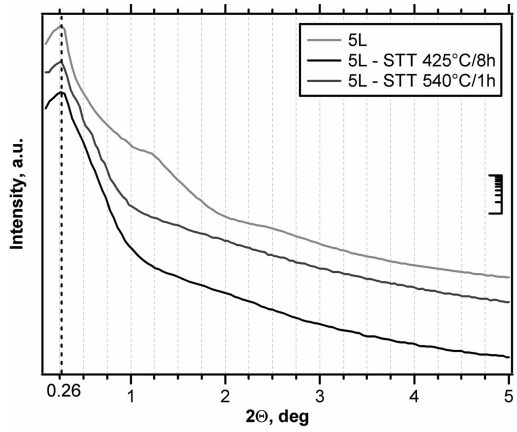

Figure 8. TiO_2 film overall density and morphology changes determined from GISAXS reflective scans. Critical angles (black dashed line) indicate the overall density of TiO_2 films to be around 1.3 g/cm^3. The logarithmic scale bar represents one order of a magnitude of counts per second.

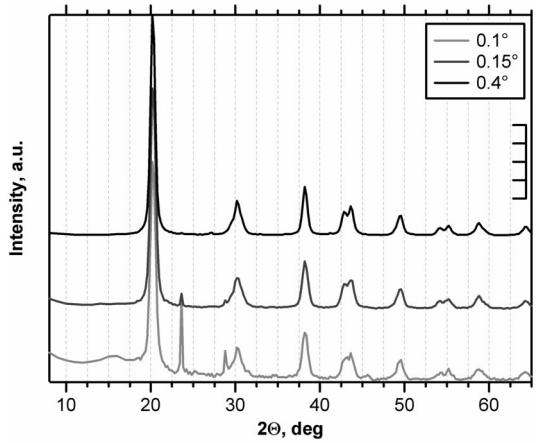

Figure 9. Diffraction patterns of the five-layer film thermally treated at 425 °C for 8 h. Scherrer calculations from scans with different penetration depths provided consistently the particle size ranging between 11−12 nm. The deeper scan (0.4°) with a higher penetration depth indicates a slight increase of the particle size in the bottom layers. The scale bar represents 20 000 counts/s.

bulk powder materials associated the peak maxima with a cubic mesophase space group ($Im\bar{3}m$) that was indexed with *d*-spacings of 7.6, 5.3 and 4.3 nm for the (110), (200) and (211) parameters, respectively.[4] The SAXS on thin TiO_2 films usually provides less detailed data, as there is limited number of peaks (often only one), evidencing just short-range ordering.[16] However, the cubic, hexagonal and lamellar phases are distinguishable in some cases. Better ordering is traceable by SAXS of films prior to calcination or after mild calcinations. Most of these studies evidenced that ordering of mesopores is perpendicular to the surface.

On the basis of our GISAXS results supported by other analytical data, the indexes might actually be a perfect fit for the TiO_2 particle size (7.6 nm) and the intermediate distance between particles with two medians at 5.3 and 4.3 nm. This conclusion matches a general rule in sintering of spherical particles that the pore size corresponds to approximately half of the particle size.

Figure 4A and B describes our model of the morphology of the P123 templated structure. We assume that the organization of particles is random. However, the close packing of the fused particles on the P123-originating pores makes the structure looking regular. Analogously to the inversion opal,[22] the pores in the bulk are surrounded by the framework of titania, while directly on the surface the ex-micelles form holes. We proportionally overlaid the model of 8 nm particles on 20 nm pore with a SEM picture of a real structure in Figure 4C. The projection of this model to the actual structure is quite satisfactory.

The particle size of 8−10 nm and the pore size were verified by number of methods. TEM pictures (Figure 2C and D) and SEM images (Figure 3A) confirm the average primary particle and pore size determined from GISAXS (8.9 nm particle and 18 nm pore size on the surface). The particle size agrees well with the references,[7,8,23,24] but others have also reported on considerably smaller anatase particles

(22) Kavan, L.; Zukalova, M.; Kalbac, M.; Grätzel, M. *J. Electrochem. Soc.* **2004**, *151*, A1301.
(23) Liu, K.; Zhang, M.; Shi, K.; Fu, H. *Mater. Lett.* **2005**, *59*, 3308.
(24) Liu, K.; Fu, H.; Shi, K.; Xiao, F.; Jing, L.; Xin, B. *J. Phys. Chem. B* **2005**, *109*, 18719.

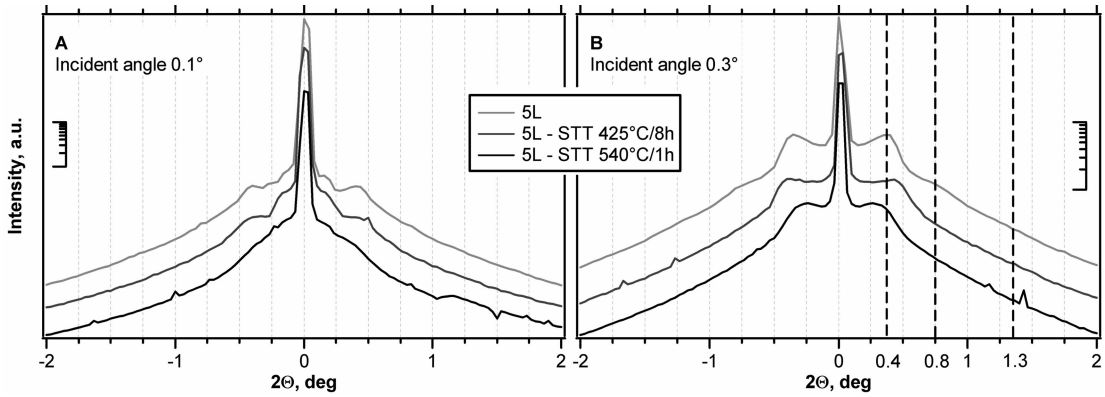

Figure 10. Comparison of GISAXS scans at incident angles (A) 0.1° (surface—low penetration depth <20 nm) and (B) 0.3° (penetrates 20−200 nm under the surface) of five-layer films with no subsequent thermal treatment and thermally treated at 425 °C for 8 h and 540 °C for 1 h. The dashed vertical lines at 0.4° (ex-P123 pore ~ 20 nm), 0.8° (particle size ~ 9 nm), and 1.3° (pore type related to the intermediate distance between particles ~ 5 nm) indicate the peak positions before the STT. The logarithmic scale bars represent one order of a magnitude of counts per second.

ranging from 2.4 to 6 nm.[4,5,25] In contrast, Sanchez et al. reported that the anatase crystal size grew from 5 to 12 nm with the calcination temperature increasing from 400 to 600 °C (4 h calcination, ramp 1 °C/min).[8]

3.2. Multilayer Film Thickness and TiO_2 Surface Area Development. As we have already shown, the large ex-micelle pore size increases stepwise from the top to the bottom layers in the TiO_2 film (Figure 1). This is due to the structure opening at the multiple calcination steps. We have observed a slight increase of the TiO_2 coherent domain size in the same direction.

Figure 5a shows adsorption isotherms of the 1 to 10 layer films. The surface area of a multilayer TiO_2 film expressed as roughness factor (Figure 5b) increases linearly up to three layers. Beyond this point, the roughness factor practically freezes at values in the range of 400−500. Above three layers, the surface area increase resulting from the deposition of a new layer is compensated by a loss of surface during the thermal processing at 350 °C (sintering of the underneath layers). In contrast, the thickness of the film increases linearly with the deposition of each additional layer.

Progressive improvement of the nanoanatase crystallinity has been observed above three layers in contrary to the stagnation of the surface area. This also is caused by the multiple thermal treatments upon deposition of each additional layer.

Five layer films (5L) with 1.3 μm standard thickness and roughness factor between 410 and 430 have been selected for the subsequent thermal treatment (STT) experiments.

3.3. Film Morphology Changes after Subsequent Thermal Treatments (STT). The intention of STT was to improve the crystallinity of nanoanatase, while preserving the highly porous morphology of the P123 templated TiO_2 mesoporous films. The electrochemistry of Li-insertion turned out to be a particularly suitable method for the investigation of nanoanatase in the presence of trace amounts of other phases (including amorphous titania and TiO_2(B)).[9,18] The electrochemical characterization (cyclic voltammograms) in Figure 6 evidence a fast conversion of TiO_2(B) into the anatase above 500 °C. Complete conversion of the TiO_2 into anatase can be also achieved by a calcination at 450 °C for 40 h.[26]

The five-layer TiO_2 films were exposed to the thermal treatments in the air at 425 °C for 8 h and 540 °C for 1 h (below and above the full conversion of TiO_2 into anatase). The morphology changes, particle size growth, porosity redistribution, collapse of the structure, and other occurrences were monitored and the results are summarized in Table 1.

Morphology changes during the subsequent thermal treatments are shown in Figure 7, which compares the results of AFM and SEM analyses. Both methods display the development of the particle size, fusion and collapse of the P123-originating porosity. Structure of the film thermally treated at 425 °C for 8 h turned into parallel patterns of particles (Figure 7B). The structure had not existed before the STT, thus it cannot be directly associated with the organization of particles caused by the P123-templating (Figure 7B). Apparently, our model of particles competing during the fusion process seems to be more appropriate.

Annealing at 540 °C for 1 h has created an open structure with broad particle and pore size distributions (Figure 7C). The P123-originating porosity has practically disappeared. Figure 7C shows large pores created by the collapse of the ex-P123 porosity. The large pore size distribution is ranging from 30 to 70 nm with the maximum at 45 nm as determined from GISAXS. The pore size distribution related to the intermediate distance between particles is also very broad with three GISAXS maxima at 17, 10, and 6 nm. Changes in patterns of the GISAXS reflective scans in Figure 8 indicate disappearance of the original structure at elevated temperature. The "critical angle" determined from these scans is often used as a film density indicator. In our case, it has remained constant at 1.3°. This is in agreement with the film thickness that also remained constant at 1.3 μm. If the film had densified, the critical angle would have increased. A critical angle value of 1.64° was received for a dense TiO_2 layer with no porosity.

Data in Table 1 confirm a significant drop of the film roughness factor as a result of STT. The drop of roughness

(25) Bartl, M. H.; Puls, S. P.; Tang, J.; Lichtenegger, H. C.; Stucky, G. D. *Angew. Chem.* **2005**, *119*, 3099.

(26) Kavan, L.; Rathousky, J.; Grätzel, M.; Shklover, V.; Zukal, A. *J. Phys. Chem. B* **2000**, *104*, 12012.

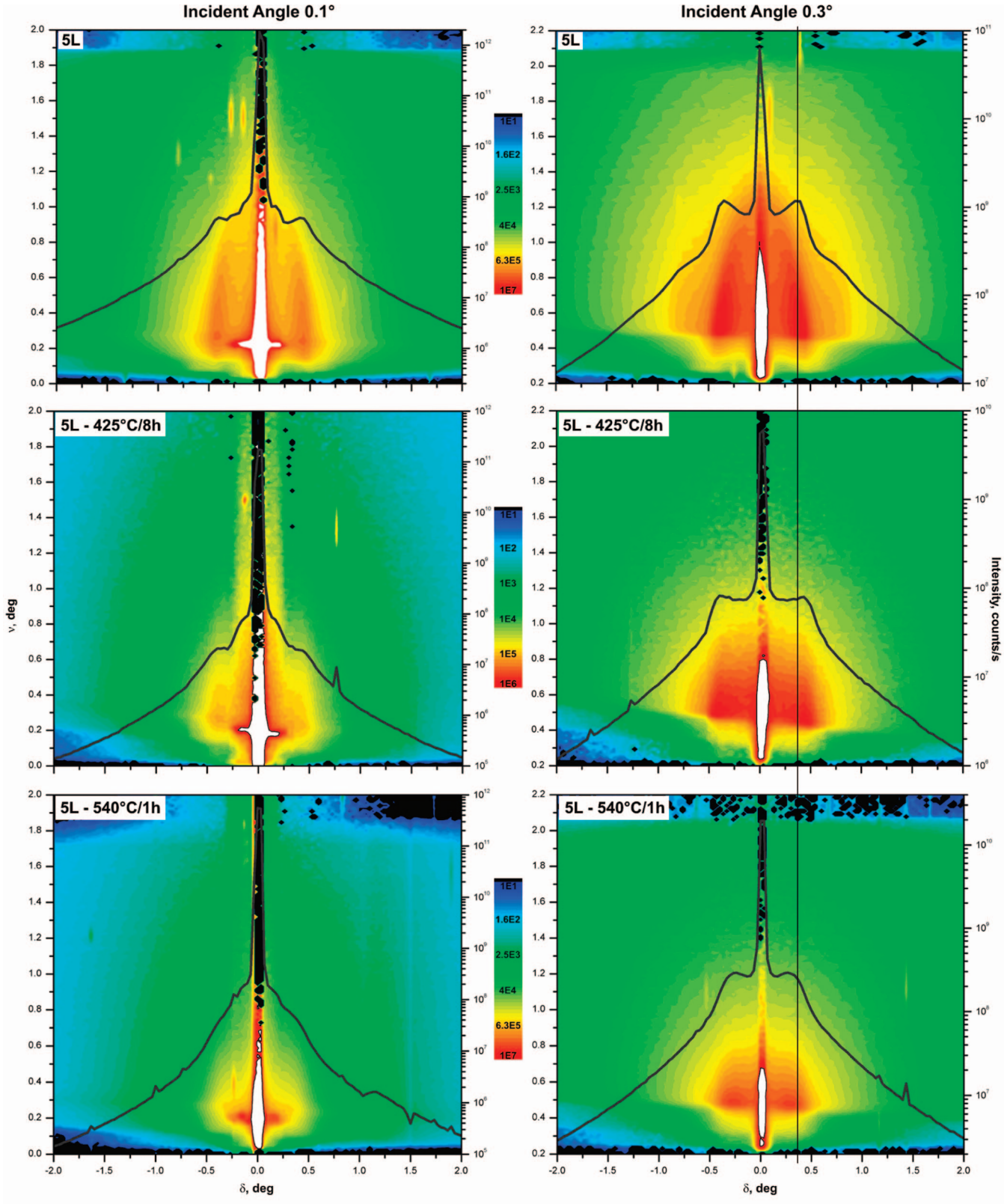

Figure 11. GISAXS detector maps at 0.1° (surface—low penetration depth) and 0.3° (penetrates 20−200 nm under the surface). The maps describe the morphology changes occurring during the STT. The vertical line on the right indicates the starting point of the ex-P123 pore diameter. It is followed by a shift to a smaller pore size at 425 °C and finally opening of the structure and a significant increase of the pore size.

factor from 429 to less than 100 indicates an extensive fusion, while the critical angle and film thickness indicate neither an overall density change of the film (Table 1), nor its collapse in one direction as reported previously.[9] This means that the morphology changes inside the film occur at a constant volume. Images in Figure 7 illustrate the particle sintering and growth during the STT. While the particles fuse together and the interparticle pores disappear, the relatively large ex-P123 pores are less influenced by the fusion and the film thickness remains almost intact. Redis-

tribution of the TiO_2 mass and porosity of the structure during the STT occur within the same volume.

The surface area of TiO_2, expressed as roughness factor, decreased to one-fourth at 540 °C compared to that before the STT. The average particle size increased approximately three times. The sintering proceeded slower at 425 °C. The particle size determined from GISAXS measurements was 11.8 nm at this temperature. Figure 9 displays diffraction patterns (WAXS) of the 425 °C treated film at different penetration depths. The origin of two sharp extra peaks in the surface scans is not clear. The coherent domain size from these patterns was calculated using the Scherrer equation. The obtained values of 11−12 nm are in accordance with the SEM and AFM observations. The P123-originating type of porosity seems to be partially preserved at this temperature although the pore size has shrunk from approximately 20 nm to about 15 nm (Table 1) and additional morphology changes are apparent. The originally mostly hexagonal morphology has turned into a structure consisting of curved parallel ropes of particles (Figure 7B). The pattern looks as an organized configuration, however, possessing a different morphology than the previous structure.

Besides the P123-originating pores with the main GISAXS peak around 15 nm, we have received trimodal subporosity of 6.8, 5.7, and 4.8 nm at 425 °C. These values correspond to a half of the particle size (11−12 nm). The collapse of the ex-P123 pores further proceeds with increasing temperature and it is nearly complete at 540 °C. After 1 h at this temperature, the average particle size grew to 20−25 nm, fusing into even larger aggregates. The originally complicated structure with many parameters fused into a framework with broad particle and pore size distributions. The 20 nm primary particles are often aggregated in larger clusters.

Figures 10 and 11 compare the changes before and after the STT directly on the surface (left) and throughout the top layer (right) as detected by GISAXS. All corresponding parameters are summarized in Table 1. After STT at 425 °C for 8 h, the ex-P123 pores shrink and reorganize. It is obvious that the structural changes on the surface are more dramatic than in the bulk. While there is hardly any detectable pore size maximum on the surface after the STT at 540 °C for 1 h, the bulk is not completely averaged out and still shows some regularities. The structure sinters all together and the pores open wide, approximately doubling their size. The line crossing the Figure 10 and 11 helps to emphasize these changes.

4. Conclusions

We have determined the main parameters of the P123-templated TiO_2 structure and limitations of the repeated dip coating and calcination procedure for manufacturing of multilayer films made of mesoporous TiO_2. The sintering process reducing the surface area of TiO_2 and increasing the pore and particle size in the bottom layers was described in detail. The three-layer films prepared by means of repeated dip coating exhibit the maximum surface area achievable by this method. It was impossible to further increase the surface area by deposition of additional layers; however, the nanoanatase crystallinity of the bottom layers was improved by addition of new layers and their thermal processing at 350 °C. The five-layer film represents an optimum providing both the sufficient surface area and good anatase crystallinity.

New model of the formation of the ordered structure based on particles competing for the TiO_2 matrix during the sintering process has been introduced. The P123 copolymer gives the structure the required porosity, but it does not seem to organize the particles in a certain oriented way.

The shells consist of randomly distributed TiO_2 nanoparticles. However, a number of morphologies can be achieved during the fusing process by adjustments of thermal treatment conditions. The growth of particles during their crystallization process seems to form a variety of ornamental structures depending on the calcination temperature and the TiO_2 particle size. This is especially noticeable on the film surface, where the sintering is constrained in one direction creating a denser crust layer parallel to the substrate.

This study investigated the possibility of improving the crystallinity of nanoanatase by subsequent thermal treatments at temperatures higher than 350 °C used in the manufacturing process. The experiments were performed in the range of 425−540 °C, and we have monitored the particle size growth and morphology development during the subsequent thermal treatments.

The collapse of the surface area at temperatures above 500 °C significantly limits the heat treatment as the method to further develop the anatase crystallinity. Even if the loss of the surface area was partially compensated by the improvement of the anatase crystallinity, it is unlikely that temperatures above 450 °C would be feasible for preparation of the TiO_2 structure, unless doping is used.

Subsequent thermal treatment at 425 °C does not produce phase pure anatase; however, it seems to be a reasonable compromise combining the still sufficient film surface area (roughness factor) and almost developed nanoanatase crystallinity.

Acknowledgment. This work was supported by the Czech Ministry of Education, Youth and Sports (contract No. LC-510 and COST D35 1P05OC069), and the European Commission (contract No. STRP 516982). The support from the European Synchrotron Facilities in Grenoble is greatly appreciated.

CM071452E